

Carbon nanotube plectonemes

Alireza Shahabi and Moneesh Upmanyu*

Group for Simulation and Theory of Atomic-Scale Material Phenomena (stAMP),

Department of Mechanical and Industry Engineering,

Northeastern University, Boston, Massachusetts 02115, USA. and

Department of Bioengineering, Northeastern University, Boston, Massachusetts 02115, USA.

We use all-atom computations to explore supercoiled conformations in individual carbon nanotubes (CNTs). Decreasing the end distance in finite length and torsionally constrained CNTs leads to spontaneous nucleation and growth of a nanotube plectoneme. We develop a stability diagram and comparisons with theoretical frameworks reveal the importance of non-local van Der Waals interactions. They stabilize the plectoneme to an extent that its tip locally kinks and then irreversibly reconstructs into a disordered yet strengthened structure that involves sp^3 bonding. In large diameters CNTs, the transitions are mediated by torsional buckling. The ability to engineer plectonemes in CNTs and related crystalline nanofilaments opens the possibility of a unique set of dynamically tunable functional properties at the nanoscale.

The conformations of soft filaments are sensitive to constraints that arise due to confinement and end conditions. In twist storing filaments such as DNA for example, the elastic energy associated with the overtwist can be further reduced by supercoiling of the filament axis [1]. Little is known about the formation and stability of such conformations in crystalline nanoscale filaments. The morphology shapes their properties, and a fundamental understanding is therefore crucial for applications that rely on these building blocks as active elements, even more so as the lengths of the as-synthesized nanofilaments approach macroscale dimensions. For example, lengths of CNTs grown via chemical vapor deposition (CVD) can be in excess of a few centimeters and are comparable to their persistence lengths for bending and twisting [2]. Conformations of these filaments are expected to have strong parallels with those of their soft semi-flexible counterparts. Indeed, coiled and double-helical shapes have been recently reported in ultralong fibrous assemblies of nanowires and nanotubes [3–5], yet the ability to control them is limited.

In this study, we use individual single-walled CNTs as model systems to explore supercoiled conformations in nanoscale crystalline filaments. All-atom molecular dynamics (MD) computations of finite length CNTs with a quenched twist density ϕ are employed to identify energy minimizing conformations for prescribed end distances z smaller than their (contour) length L , $\lambda = z/L < 1$. The net rotation $\Phi = \phi L$ between the ends is preserved. For generalized filaments so constrained, the combination of fixed end displacement and end rotation results in totally rigid loading and the partitioning of the elastic energy density preserves a global topological invariant associated with the supercoiled geometry, the Linking number Lk , given by the well-known Călugăreanu-White-Fuller theorem, $Lk = Tw + Wr$. The Twist Tw is the rotation of a material frame about the local tangent and the Writhe Wr is a measure of the bent geometry of the filament axis [6].

We study this interplay in three achiral CNTs: (3,3), (6,6) and (8,8) armchair nanotubes with diameters $D =$

0.434, 0.826 and 1.094 nm, respectively. In each case, the length of the nanotube is fixed, $L = 110.4$ nm. The CNTs are torsionally constrained in the range $Lk = 1.25 - 8.75$ which correspond to twist densities $\phi = 4.1 - 28.5^\circ \text{ nm}^{-1}$. The initially twisted configuration is generated by rotating the two ends relatively by an angle Φ that varies uniformly along the length. The ends are clamped to fix $Lk = \Phi/2\pi$ which equals the net twist Tw in the initially straight CNT. The end distance is decreased at a rate $\delta z/\delta t \approx 4$ nm/ns within room temperature canonical MD simulations performed using an AIREBO carbon-carbon potential [7–9].

Figure 1a depicts four commonly observed conformations, henceforth labeled C1-C4. Large Lk results in twist (torsional) buckling as the initial twist density is high [10]. As expected, this is more frequent at large diameters. The buckled configuration of a (6,6) CNT at $Lk = 6.25$ is shown in Fig. 1a (C1). It is stable for $\lambda \approx 1$ as the CNT is under tension due to the twist-stretch coupling [11]. Decreasing λ lowers the tension and it destabilizes into a helix (C2, Fig. 1a). The curvature of the CNT axis increases at the expense of the twist density and the extent of buckling therefore decreases (inset). Thereafter, the work done in decreasing λ increases the tortuosity of the CNT axis. Below another critical λ^* the helix develops a local instability that leads to the nucleation of a supercoiled phase, a nanotube plectoneme (conformation C3, Fig. 1a). The transition is spontaneous and subcritical as it is stabilized by van der Waal interactions between the helically coiled CNT surfaces. The torsional buckling is reduced in extent and is mostly confined to the plectoneme. The remainder of the CNT is twisted and devoid of helicity.

The CNT plectoneme is unlike the supercoiled conformations observed in soft filaments [12]. The looped terminal end is relatively smaller in extent and tightly curved over a radius of the order of the CNT diameter, i.e. it resembles a kink. It is not an artifact of the large strain rates; simulations with order of magnitude lower strain rates have no effect [9]. Smaller link densities $2\pi Lk/L$ result in large radii helices that again collapse into kinked plectonemes,

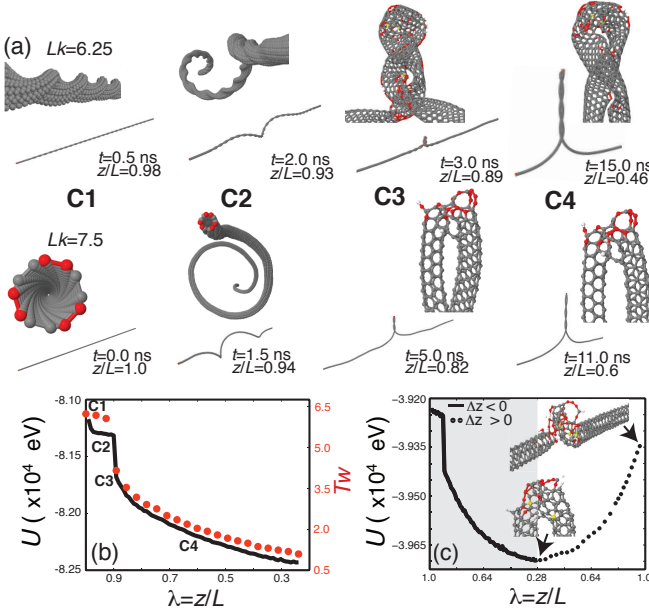


FIG. 1. (color online) (a) (top row) Sequence of configurations (labeled C1-C4) observed in MD simulations of a (6,6) CNT with Linking number $Lk = 6.25$ and decreasing end distance $\lambda = z/L$. Expanded views of the configurations are shown alongside; they are rotated to depict the details. Here and elsewhere, the atoms are colored based on the number of neighbors within a cut-off distance of 1.5 \AA : white-1, red-2, grey-3 and yellow-4. (bottom row) Same as above but for a (3,3) CNT with $Lk = 7.5$. (b) Variation in total interaction energy $U(\lambda)$ and the twist $Tw(\lambda)$ for the (6,6) CNT in (a). The locations of the configurations C1-C4 in (a) are marked. (c) $U(\lambda)$ for a (3,3) CNT with $Lk = 7.5$, for decreasing (solid curve) and increasing (dotted curve) end distance z . (inset) Magnified views of kinked tip of the plectoneme at $\lambda = 0.28$, and at $\lambda = 1$ following the re-extension [9].

suggesting that the release of the torsional energy is size constrained such that the plectoneme tip cannot form a much larger sized loop. The kink is structurally defective (inset, Fig. 1c). For clarity, the carbon atoms are colored based on their local coordination within a cut-off radius of 1.5 \AA . The changes in the bonding network include the formation of vacancy clusters and pentagon-heptagon (5-7) defects that absorb the large curvature [9]. In addition to several dangling bonds (white) and non-linearly strained atoms (red), we observe the formation of a several clusters each containing an sp^3 bonded carbon atom at its core (yellow). Further decreasing λ results in the growth of the plectoneme with concurrent elimination of the twist buckles. The defective structure of the kink remains mostly unchanged indicating that the modified bond network is stable. Away from the tip, the two CNT segments form a double helix with a radius of the order of the CNT diameter $r \approx D/2$ and a much larger pitch length, $p \approx 20r$.

Figure 1b shows the response of a (3,3) CNT with $Lk = 7.5$. The nanotube does not buckle due to its smaller radius. As before, the initially straight and twisted conformation

destabilizes into a helix (C2, $\lambda = 0.94$). The nucleation of the plectoneme is relatively delayed (C3, $\lambda = 0.82$). The looped end is small and defective with several vacancy clusters that lead to partial fracture at the kink, and dangling bonds that reconstruct into short bridges [9]. Thereafter, the supercoiled region lengthens with decreasing λ (C4) and a pitch length $p \approx 25r$.

The evolution of the interplay between the energy and geometry of the conformations is shown in Fig. 1b for the (6,6) CNT (Fig. 1a), a combined plot of the net interaction energy U and Twist Tw as a function of λ . The energy evolution $U(\lambda)$ shows four distinct regimes: i) a rapid decrease as the twisted CNT transitions into a helix, ii) a slower linear decrease as the helix increases its radius and then localizes, iii) an abrupt, large decrease at $\lambda \approx 0.9$ consistent with the spontaneous nucleation of the plectoneme, iv) and a slow non-linear decrease as the plectoneme grows. The stored twist Tw is extracted dynamically [9] and exhibits similar trends.

The initial linear decrease is due to the increasing Writhe as the helical phase forms and grows. On the other hand, the nucleation of the plectoneme leads to a larger decrease at $\lambda \approx 0.9$, followed by a gradual non-linear decrease that closely follows the change in energy as the plectoneme grows in length. The response of the (3,3) CNT is quite similar (Fig. 1c) with some minor variations that arise primarily because of the absence of buckling. Both U and Tw decrease smoothly during the transition to the helix. The transition to the plectoneme occurs at $\lambda \approx 0.9$, yet the nucleated plectoneme is longer in length and the decrease in energy (per atom) is larger as the resultant bond network consists of several sp^3 bonds. We have tested the stability of the kinked plectoneme by re-extending the CNT. The energy increases non-linearly without any discontinuities as the plectoneme unwinds. The remainder of the CNT is not helical. At $\lambda = 1$, the defective kink persists and both U and Tw (not shown) do not recover completely. Interestingly, U is lowered following re-extension as the defective region is stabilized and strengthened by the bond network.

Figure 2 shows the evolution of the plectoneme post-nucleation. The pitch length $p(\lambda)$ is not constant, rather it increases for both (3,3) and (6,6) CNT. The increase is linear, $p \sim \lambda$, although the response for the (6,6) CNT is more rapid as it is buckled. Evidently, the plectoneme becomes less intertwined as it grows, and this indicates that i) the CNTs slide with respect to each other, and ii) there is no twist stored within the plectoneme [9]. A simple analysis yields insight into the stability of the plectoneme; in the absence of twist and stretching strains within the plectoneme, the energetics reduces to a competition between bending and interaction energies and the work done by the external couple. The bending energy scales as $U_b(p) \sim (D^2 \kappa_b / p^4) l$ while the interaction energy scales as $U_i(p) \approx (au_0) l + \mathcal{O}(p^{-2})$, where κ_b is the bending rigidity, u_0 is the interaction energy per unit

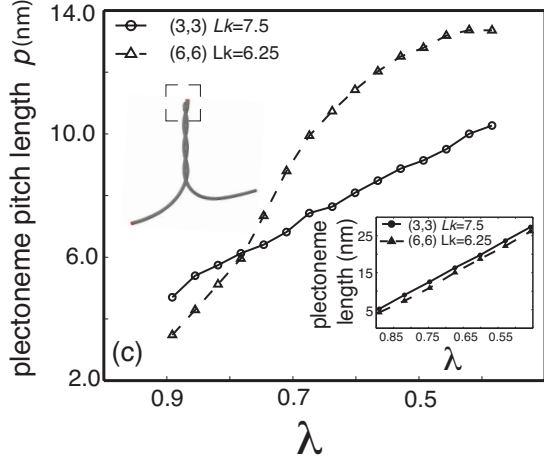


FIG. 2. The evolution of the pitch length p of the plectoneme with decreasing λ in supercoiled CNTs shown in Fig. 1. (inset) Variation in the tip-to-base plectoneme length with λ .

area between graphene elements and a is the width of the approximately straight interaction area for the large p/r ratios observed here [13, 14]. The base-to-tip plectoneme length also grows linearly, $l \sim \lambda$ (inset). Ignoring changes in the kink structure and the curvature of plectoneme base that connects to the ends, the energy stored in the double helical region evolves as $U \sim D^2 \kappa_b / \lambda^3 - a u_0 \lambda$. For CNTs, $k_b/u_0 > 1$ and $a \sim r$ [15]. Clearly, the interaction energy is insufficient and the double-helical segment is stabilized by the external work done by the tension $T(\lambda)\lambda$ and the release of the torsional energy $M(\lambda)\phi$.

In order to develop a more complete picture of the stability of and transitions in the conformations, we plot the response of several achiral CNTs with varying Lk as a dimensionless conformational phase diagram, λ versus the size-weighted link density, $\zeta = 2\pi Lk(D/L)$ (Fig. 3). The two solid boundary lines define regions associated with the stability of the three conformations - twist, helix, and plectoneme. The region enclosed by the dashed line (top right) indicates completely or partially buckled conformations at larger CNT diameters and Lk , as expected. The twist-helix transition occurs for $\lambda \approx 1$ and it is independent of the link density ζ . Evidently, the twist is stabilized by large axial tension which decreases linearly with λ , as confirmed later (Fig. 4b). Below a critical tension, the helix is energetically preferred. At large Lk , the transition is mediated by buckling of the nanotube which lowers the critical λ for the transition. The helix-plectoneme transition varies dramatically. The critical point λ^* increases with the critical link density ζ^* and then saturates as we approach the buckling threshold. The trend is as expected since the localization of the helix that results in the plectoneme is facilitated by the initial twist. To develop a more detailed understanding, we follow the energetic analysis performed by Coyne [16] on a finite-length elastica subject to an end couple (M , T).

Minimization of the energies stored in bending and twisting and the work done by the end tension (for fixed Lk there is no work done by the moment) as a function of the end displacement, the critical point (T^* , β^*) at which the helix transitions into a localized loop is [16]

$$T = \frac{\kappa_t^2}{4\kappa_b L^2} \frac{(\phi L - 4 \sin^{-1} \beta)^2}{1 - \beta^2}, \quad (1)$$

where κ_t is the torsional rigidity and β is a dimensionless end displacement defined as $\beta = d\sqrt{T/16\kappa_b}$. Figure 4a shows the theoretically predicted $T(d, Lk)$ for an (8, 8) CNT. For fixed Lk , the curves $T(d)$ are bistable and the nose of each curve where the helical and the localized loop (precursor to the plectoneme) meet is the critical point for the transition [17]. For comparison, we have also plotted the solution for an infinitely long planar looped elastica, $T = 16\kappa_b/d^2$, which overestimates the critical tension; the difference δT increases quadratically with Lk (inset). Combining the planar solution with this correction yields a general solution for the critical tension $T^*(d^*, \zeta^*)$ [9]. The critical points $\lambda^* = 1 - (d^*/L)$ and ζ^* are plotted in the phase diagram (inset, Fig. 3). The trends are similar but do not agree quantitatively. Refinements such as the effect of clamped edges and more detailed analyses that absorb the shape of the plectoneme [18] can mitigate the discrepancy, yet the fact that the theory overestimates the critical end distance and link density suggests a non-trivial effect of long-range interactions that are ignored in these classical

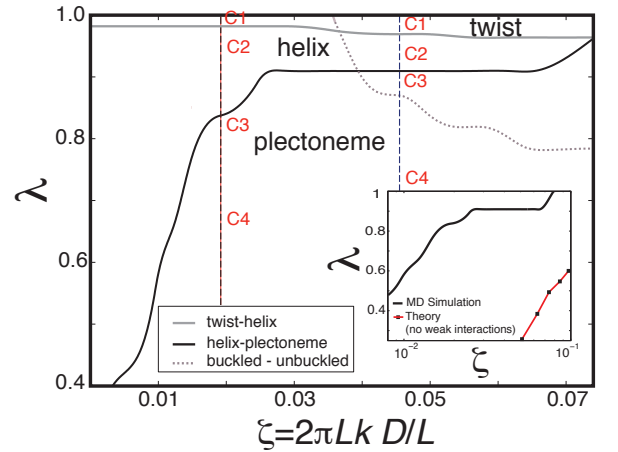


FIG. 3. Dimensionless conformational diagram for CNTs with varying diameters D and Linking numbers Lk . The solid curves represent co-existence lines for the three phases observed in the simulations: twist, helix, and plectoneme. Torsionally buckled CNTs are stable above the dotted curve (high ζ and λ). The blue and red vertical lines correspond to the achiral CNTs shown in Fig. 1: (3,3) with $Lk = 5$, and (6,6) with $Lk = 6.25$, respectively. The points at which configurations C1-C4 reported in Fig. 1 first appear are also indicated. (inset) The helix-plectoneme transition observed in the simulations and that predicted by theory for non-interacting elastic filaments [16]; see text for details.

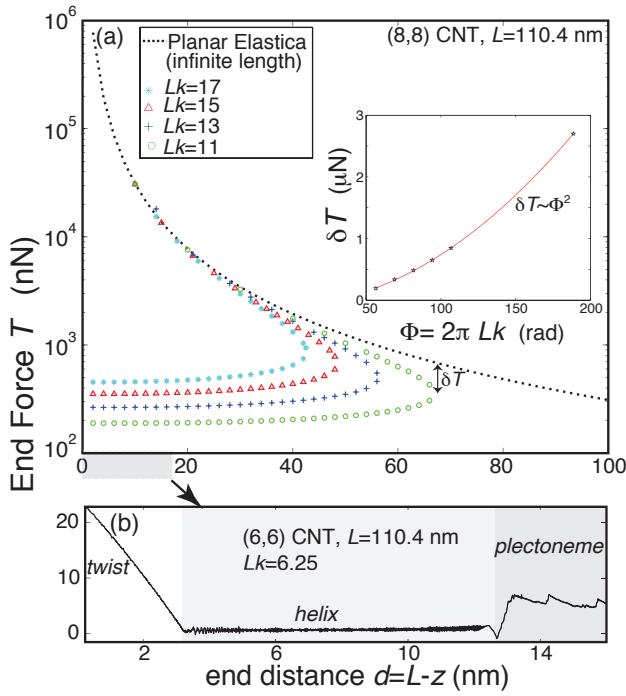


FIG. 4. Theoretical force-displacement curves based on Eq. 1 for the (8,8) supercoiled CNT and varying Lk [16]. The lower arm in each curve is the helical phase and the upper arm is that localized instability that leads to plectoneme nucleation. The tip of the curves is the critical point (T^* , d^*) for the helix-plectoneme transition. The dashed line is the planar-looped elastica solution for an infinite elastic rod. (inset) The correction to the planar-looped elastic solution δT for the critical point as a function of Lk .

elastica solutions and enhance the plectoneme formation. As an analogous example, recent analyses of DNA supercoiling reveal that incorporating the electrostatic interactions within the supercoil improves the agreement with experiments [19].

In order to quantify this effect, we extract the end tension dynamically for the (6,6) CNT with $Lk = 6.25$ (Fig. 4b). The tension, of the order of tens of nN, is smaller compared to the plots shown in Fig. 4a as the Lk is itself smaller. The twist-helix transition follows the linear decrease in the tension which then stabilizes to a few nN. The localized instability results in an abrupt decrease in the tension, large enough to change its sign. The transition occurs at almost constant λ and the growth of the double-helix is reined in by the abrupt increase in the tension that eventually exceeds that in the helical phase. Thereafter, the tension varies in a serrated fashion for every new loop absorbed by the plectoneme. These transitions are gradual, and each cycle involves a balance between long-range interactions that facilitate loop formation followed by recovery of the tension as the plectoneme grows and adjusts its pitch length.

In conclusion, we present strategies for engineering plectonemic phases in individual carbon nanotubes. Our results have implications for supercoiled conformations

in nanoscale crystalline filaments such as nanowires and nanoribbons where the combination of crystalline order and long-range attractive interactions is equally important. Although details of the plectoneme structure await experimental confirmation, their controlled nucleation and growth opens up the possibility of a unique set of multifunctional properties - electronic, mechanical, thermal, optical - that remain to be harnessed in nanofilament-based device platforms. More importantly, the quantitative understanding developed in this study allows control over the extent of supercoiling that translates to *on-demand* and reversible modulation of these properties, a key enabler for robust and highly non-linear transport, actuation, switching and energy storage at the nanoscale.

Acknowledgements: The computations were performed on *stAMP* and *Discovery* (MGHPCC) supercomputing resources at Northeastern University.

* mupmanyu@neu.edu

- [1] T. R. Strick, J. F. Allemand, D. Bensimon, and V. Croquette, *Biophys. J.* **74**, 2016 (1999); J. D. Moroz and P. Nelson, *Macromolecules* **31**, 6333 (1998).
- [2] L. X. Zheng et al., *Nature Mat.* **3**, 673 (2004).
- [3] Y. Wang et al., *J. Amer. Chem. Soc.* **133**, 20060 (2011).
- [4] M. D. Lima et al., *Science* **338**, 928 (2012).
- [5] Y. Shang et al., *ACS Nano* **7**, 1446 (2013).
- [6] G. Călugăreanu, *Czechoslovak Math. J.* **11**, 588 (1961); J. H. White, *Am. J. Math.* **91**, 693 (1969); F. B. Fuller, *Proc. Natl. Acad. Sci.* **68**, 815 (1971).
- [7] D. W. Brenner, O. A. Shenderova, J. A. Harrison, S. J. Stuart, B. Ni, and S. B. Sinott, *J. Phys.: Cond. Mat.* **14**, 783 (2002).
- [8] S. J. Plimpton, *J. Comp. Phys.* **117**, 1 (1995).
- [9] See Supplemental Material at [URL] for details.
- [10] Q. Wang, S. T. Quek, and V. K. Varadan, *Phys. Lett. A* **367**, 135 (2007).
- [11] H. Y. Liang and M. Upmanyu, *Phys. Rev. Lett.* **96**, 165501 (2006).
- [12] T. C. Boles, J. H. White, and N. R. Cozzarelli, *J. Mol. Biol.* **213**, 931 (1990); A. Bancaud et al., *Nature Struct. Mol. Biol.* **13**, 444 (2006); A. Ghatak and L. Mahadevan, *Phys. Rev. Lett.* **95**, 057801 (2005).
- [13] H. Y. Liang and M. Upmanyu, *Carbon* **43**, 3189 (2005).
- [14] B. Pokroy, S. H. Kang, L. Mahadevan, and J. Aizenberg, *Science* **323**, 237 (2009).
- [15] L. A. Girifalco, M. Hodak, and R. S. Lee, *Phys. Rev. B* **62**, 13104 (2000).
- [16] J. Coyne, *IEEE J. Oceanic Eng.* **15**, 385 (1990).
- [17] J. M. T. Thompson and A. R. Champneys, *Proc. Roy. Soc. London A* **452**, 117 (1996); G. H. M. van der Heijden and J. M. T. Thompson, *Nonlinear Dynamics* **21**, 71 (2000).
- [18] S. Goyal, N. Perkins, and C. Lee, *J. of Comp. Phys.* **209**, 371 (2005); P. K. Purohit, *J. Mech. Phys. Solids* **56**, 1715 (2008).
- [19] N. Clauvelin, B. Audoly, and S. Neukirch, *Biophys. J.* **96**, 3716 (2009).